Study of Surface Wind and Mean Square Slope Correlation in Hurricane Ike With Multiple Sensors

Scott Gleason ⓘ, *Senior Member, IEEE*, Valery U. Zavorotny ⓘ, *Fellow, IEEE*, Dennis M. Akos ⓘ, Sara Hrbek, Ivan PopStefanija, *Member, IEEE*, Edward J. Walsh, *Senior Member, IEEE*, Dallas Masters, *Member, IEEE*, and Michael S. Grant ⓘ

Abstract—This paper analyzes and compares multiple techniques for estimating the mean square slope (MSS) of surface waves during Hurricane Ike in the Gulf of Mexico and studies the correlation of the MSS estimates with wind speed measurements along the same tracks. Three separate instruments collected measurements in parallel, including a GPS reflectometry (GPS-R) receiver, a stepped frequency microwave radiometer (SFMR), and a wideswath radar altimeter (WSRA). These datasets were used to study the correlation between the flight level and near-surface wind and MSS during Hurricane Ike in 2008. The GPS-R, SFMR, and WSRA instruments recorded temporally and spatially coincident data during two passes over the hurricane eye. This paper estimates the ocean surface MSS using GPS-R for two eye transects using: a least squares model fitting technique, the reflected signal waveform width, and an integration of the reflected signals in an area around the peak. Subsequently, the correlations between the GPS-R and WSRA MSS estimates and the SFMR wind speed estimates are compared to reveal regions of high and low surface MSS to wind speed correlation. Finally, a relationship between wind and MSS was derived from the GPS-R and SFMR data and is compared to existing MSS/wind models, including the results obtained by Katzberg *et al.* for hurricane conditions.

Index Terms—Geophysical measurements, global positioning system, microwave reflectometry, radar altimetry, remote sensing, sea surface, sea surface electromagnetic scattering, wind.

I. Introduction and Background

THE mean square slope (MSS) of wind-driven waves in hurricanes is an important quantity for understanding the physical processes at the air–sea interface and for verifying new advanced models of hurricane development [1]–[3]. However, *in situ* MSS measurements in hurricanes do not exist, and the MSS data obtained from existing remote sensing techniques are rare and difficult to obtain [4], [5]. Recently, the bistatic radar scatterometric technique has been increasingly employed for measurements of ocean winds and MSS using global navigation satellite system (GNSS) scattered signals [6]–[8]. The estimation of near-surface winds and their relationship to surface MSS in hurricanes is of critical importance to the NASA Cyclone GNSS (CYGNSS) mission, which relies on GNSS reflected signals to estimate winds in hurricane conditions [9]. Understanding the relationship between surface MSS and near-surface wind in a dynamic storm is directly relevant to the CYGNSS wind speed estimation algorithms [10], [11]. The wind to MSS model used by CYGNSS assumes that the MSS and wind are highly correlated [12]. In a rapidly changing hurricane, this assumption may break down as small scale storm dynamics cause winds and the corresponding surface MSS to diverge from a highly correlated relationship [13], [2], [14]. This paper estimates MSS using GPS reflections and calculates how these estimates correlate with wind speed estimates from stepped frequency microwave radiometer (SFMR) and flight level winds.

After a brief introduction on hurricane wind and wave sensing using GPS, an overview of the aircraft overflight of Hurricane Ike and a description of the GNSS bistatic radar together with the other instruments are presented in Section II. Section III describes the GPS data collected and its calibration using a nearby dropsonde estimated wind, deployed from the same aircraft. Section IV presents the results of MSS estimation using a least squares MSS estimation technique with a GPS reflectometry (GPS-R) forward model. Section V explores the correlation between least squares GPS-R estimated MSS and SFMR and flight level wind measurements. Section VI explores the use of alternative GPS-R waveform parameters in the retrieval of surface MSS, including the waveform width and integral methods and correlates these MSS estimates with SFMR winds. Section VII presents the comparison of the wide swath radar altimeter (WSRA) and GPS-R MSS measurements. Section VIII derives an MSS to wind speed function and compares the GPS-R versus SFMR results derived here to the MSS-to-wind model developed in [15]. Section IX includes a brief summary.
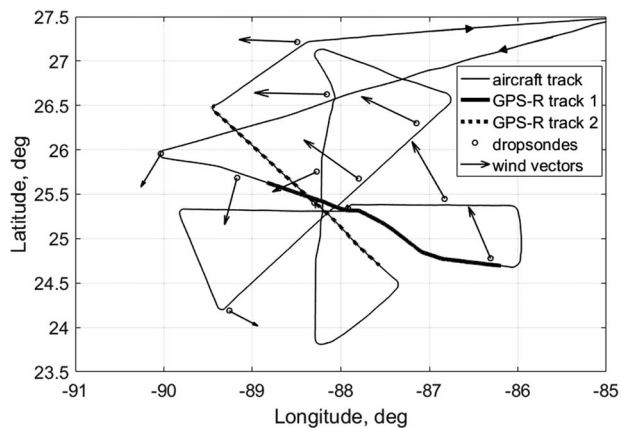
Fig. 1. NOAA aircraft ground track on September 11, 2008. Thick solid and dashed lines indicate the two GPS-R data-collection tracks. Dropsonde at $[25.54, -89.2]$, slightly before start of track 1, used as calibration reference wind speed.

A. History of GNSS-R Wind and Wave Sensing

Using GPS signals in a forward scattering configuration for remote sensing was first proposed by Hall and Cordy in [16]. Subsequently, the concept of a passive reflectometry and interferometry system altimetry was put forward by Martin-Neira in [17]. Several years later, the first demonstration of wind sensing using GPS reflections was carried out by Garrison *et al.* in [18]. Additionally, several other researchers have performed experiments from near-earth and space platforms for wind or wave sensing: [6], [11], [19]–[23]. Together, the work of these researchers established that GPS signals could be used to sense the near-surface ocean wind and wave conditions from aircraft and spacecraft altitudes. Notably, a group led by S. Katzberg performed several experiments to estimate surface winds and MSS in hurricanes [15], [24]–[26]. These results and others (see, e.g., references in [8]) were key to demonstrate the feasibility of the NASA CYGNSS hurricane observing satellite mission, launched in 2016 [9]. A summary of the GPS-R technique and its applications can be found in [7] and [8].

II. EXPERIMENT SUMMARY AND DATA COLLECTION TRACKS

The data used in this research were all collected on a single NOAA P-3 aircraft flight through Hurricane Ike on September 11, 2008. The flight originated from MacDill AFB near Tampa, FL, USA, and made multiple passes over Hurricane Ike in the Gulf of Mexico. The aircraft flew through the hurricane at about 2500 m height, performing a characteristic flight pattern comprised of several radial lags that traversed the hurricane eye at different azimuthal angles and covering a 300 by 300 km area under various sea-state conditions (see Fig. 1). Buoys and aircraft measurements indicated that the wind speed varied between 5 and 50 m/s, with wind directions as expected for a tropical cyclone.

A. Stepped Frequency Microwave Radiometer

The aircraft was equipped with an SFMR, which is a C-band remote sensing instrument that is routinely flown into hurricanes
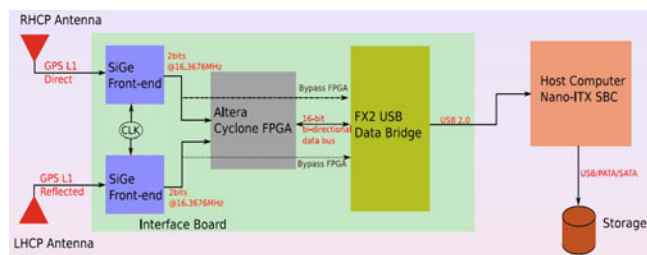

Fig. 2. Block diagram of the CUBR.

by NOAA to measure surface wind speed and rain rate [27]. These measurements provided a comparison wind speed for analyzing the correlation between estimated MSS and wind along the two measurement tracks in which GPS data were collected.

B. Wide Swath Radar Altimeter

A NOAA Ku-band WSRA was mounted on the same aircraft [28]. This unique airborne system was developed by ProSensing to provide observations of the sea surface MSS and rain. The WSRA data are processed on the NOAA P-3 hurricane research aircraft and transmitted to the National Hurricane Center to support the NOAA hurricane operations and research missions. More information about the design and operation of the WSRA can be found in [28]. The WSRA provides near-real-time reporting of ocean directional wave spectra, significant wave height (SWH), rain rate, and the MSS of the ocean surface originating from the wave spectra limited by the high frequency cutoff corresponding to the Ku frequency. The WSRA sensor MSS algorithm uses the Ku-band radar backscattered power falloff with incidence angle to estimate the MSS of the ocean surface. More details on this MSS retrieval can be found in [29].

C. University of Colorado GNSS Bistatic Radar

The aircraft carried a GNSS bistatic radar built by the University of Colorado and a NASA Langley GPS reflections receiver (GPSRS), both interfaced to the same nadir GPS antenna. Details of the Langley GPSRS receiver can be found in [30] and [31].

The CU GNSS bistatic radar (CUBR) instrument is essentially a data logger that collects and stores down-converted raw intermediate frequency (IF) GPS samples. It makes use of dual isolated GPS L1 radio application-specific integrated circuit components, which have been clock synchronized to capture the raw IF streams from both nadir and zenith antennas mounted on the aircraft. The bandwidth of the captured data is approximately 2.2 MHz (which is determined by the radio frequency (RF) front-end configuration), with a down converted IF frequency of 4.092 MHz (from the original transmitted GPS L1 carrier frequency of 1575.42 MHz). The sampling frequency is 16.3676 MHz, and 2-b data are collected from zenith and nadir channels. This receiver configuration is sufficient to fully capture the reflected signals with negligible loss, as explained in detail in [32]. The block diagram of the system is shown in Fig. 2.
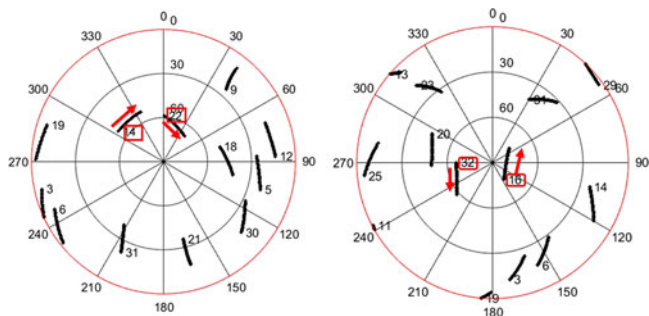
Fig. 3. Azimuth-elevation plots of all visible satellites for two GPS-R intervals: 10:02–10:42 UTC and 14.16–14:56 UTC. Pairs of satellites at high elevation angles are singled out by red boxes. Arrows show the heading direction for the satellites on the sky.
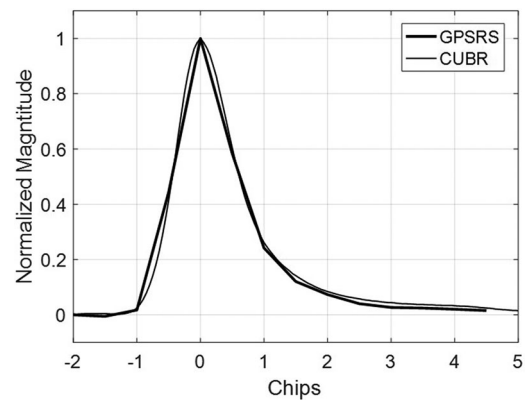

Fig. 4. Comparison of example set of 1-s waveforms averaged over 10 s from the NASA Langley and Colorado University receivers. The NASA Langley receiver (GPSRS) processes one signal in real time at 0.5 chip delay spacings, whereas the University of Colorado instrument (CUBR) generates sample data processable on the ground to any delay bin spacing and any PRN.

The data collection with the CU bistatic radar took place during two intervals referred to as "track 1" and "track 2" throughout this paper. Track 1 (solid bold) and track 2 (dashed) are shown in Fig. 1. The start time of the track 1 collection was approximately 10:02–10:42 UTC, whereas the start time of track 2 was approximately 14:16–14:56 UTC.

Even though up to 12 GPS satellites were visible from the aircraft, only a pair of GPS satellites at high elevation angles were used for each track to avoid complications from higher incidence angle scattering effects, where the signal can spread over several tens of kilometers on the surface. This also served to minimize the changes in the reflection geometry over the track and corresponding changes in the receiver antenna gain.

For track 1, pseudorandom noises (PRNs) 14 and 22 were processed, and PRNs 16 and 32 were processed for track 2. Here, the PRN code modulated onto the signal of the transmitting GPS satellite is used to uniquely identify the satellite during processing. These satellites were chosen given their relatively high elevation angles (near or above $60°$). Generally, the observed waveforms between the two different reflections for a given track are similar, and for the plots shown below the MSS retrievals for the two PRNs are averaged together. The geometry as displayed on a "sky plot" of the two PRNs for each of the two tracks is shown in Fig. 3.

The receiver included the following:
1) two GPS L1 frequency low-gain antennas, a zenith-looking right-hand circular polarized antenna for direct signals, and a nadir-looking left-hand circularly polarized antenna for reflected signals;
2) a low-noise amplifier (LNA); and
3) an RF front end, which down converted the signals from GPS L1 to IF.

The sampled raw IF data was then logged from both the direct and reflected channels to a large solid-state hard drive for ground processing (see Fig. 2).

The advantage of this raw IF sampling instrument is that it allowed the postprocessing of reflected waveforms on the ground to very high delay resolution, as well as the processing of multiple GPS satellites in view. We will demonstrate in the following that the measurements from the CU bistatic radar and the Langley GPSRS are consistent.

D. GNSS Bistatic Radar Data Processing

The raw data collected with the GNSS bistatic radar on board the NOAA P-3 aircraft have been postprocessed on the ground to obtain the delay waveforms of the surface-reflected signals using a software-defined radio system described in [33]. The first step in processing performs a cross correlation of the recorded raw data with a replica of the PRN code of the GPS satellite for a set of different time lags. The value of the reflected signal carrier frequency offset was chosen to compensate for the reflected signal Doppler shift associated with the nominal reflection point on the earth surface. The cross correlation is achieved by performing a coherent integration over an integration time, $T_{\text{coh}} = 1$ ms, that is short enough to neglect the decorrelation of the surface-reflected signal since the correlation time of the speckle noise caused by surface scattering is about 5 ms, estimated in [34]. These signals were processed into delay waveforms at 0.05 chip delay bin spacing. The individual correlation waveforms were noisy due to speckle and required further incoherent averaging. The incoherent averaging time used to generate waveforms for the MSS estimation algorithm was 1 s. We considered this choice of averaging time optimal, allowing us to significantly reduce speckle noise (the number of independent samples is of the order of 200–1000), and to have a satisfactory spatial resolution (~ 150 m) to discern the hurricane structure.

Examples of the reflected signal waveforms from the CU bistatic radar and the Langley receiver are shown in Fig. 4. The thin trace shows the 1-s averaged and normalized (using the maximum correlation value) waveform processed in 0.05 chip steps from the CU bistatic radar. The thick track is the averaged and normalized signal over the same time interval from the Langley receiver in 0.5 chip steps. The two signals are very similar, which is expected as both instruments were interfaced to the same aircraft antennas. This comparison was performed at roughly 5-min intervals across the track, to verify the measurement consistency between the two sets of data, and to provide a simple consistency check of the waveforms under various wind conditions used in the analysis.

III. GPS-R Delay Waveform Calibration

The postprocessed and incoherently averaged delay wave-forms generated by the CUBR instrument were calibrated from units of counts to watts before MSS estimation was performed. To accomplish this, we used a reference "truth wind" measured from a nearby dropsonde and converted this to an estimate of MSS using the Elfouhaily *et al.* wave model [37]. The calibration region was the region labeled "A" in Fig. 5, as it was determined to contain the most uniform and lowest winds along both tracks (as estimated by [35]). The estimated wind speed in the reference region was then converted to a reference MSS using the Elfouhaily *et al.* wave model. Subsequently, a set of reference model waveforms was generated using the [36] model (hereinafter referred to as the Z–V model) with the representative reflection geometry. These reference model waveforms were then anchored to the estimated MSS over the calibration region, providing a power reference magnitude for the estimated MSS values used during the waveform fitting along the entire tracks. The reference CUBR GPS-R waveforms were averaged over 2 min (1200 waveforms total, 2 min of 10-Hz waveforms) within the calibration wind region. These GPS-R waveforms along the track were then relatively scaled based on the reference power and MSS of the reference model waveform, which allow all of the CUBR instrument waveforms to be converted to units of watts, anchored to the waveforms and MSS in the calibration region. The steps in the algorithm can be summarized as follows.

1) Use the Elfouhaily *et al.* wave model to estimate the surface MSS at the dropsonde estimated wind speed in the calibration region.
2) Identify a low wind portion of the measurement track interval outside the hurricane eye: region "A" in Fig. 5.
3) Generate a series of reference model waveforms, over a complete range of MSS values, using the measurement reflection geometry.
4) Retrieve the wind speed from the dropsonde wind speed estimate available in the calibration region. Dropsonde wind was estimated within 10 min of start of GPS-R collection for track 1.
5) Select the reference model waveform that corresponds to the Elfouhaily *et al.* wave model estimated MSS. This provides a relative magnitude calibration of the power level for the reference waveform at the reference MSS in the calibration region.
6) Scale the measured waveforms across the entire track relative to the reference waveform peak power.
7) Use the sequence of calibrated waveforms over the entire track as inputs to the least squares model fitting MSS technique.

Due to some unknowns in the instrument configuration, a number of assumptions needed to be made when calibrating and estimating MSS from the GPS-R waveforms. These included the following.

1) GPS-R instrument antenna gain was relatively constant over the range of azimuth and elevation angles along the reflection track. No measured pattern information on the nadir antenna was available. However, from the specification of the antenna, we assumed a relatively constant hemispherical pattern as a function of incidence and azimuth viewing geometry. From an analysis of the reflection geometry for all four satellites tracked, the change in incidence angle was never more than $10°$. This small change together with the higher elevations of the chosen satellites minimized the error introduced due to the unknown changes in antenna gain over the measurement tracks. Nonetheless, these uncorrected variations of antenna gain are a potential source of error in the results.
2) The gain and noise figure of the GPS-R LNA remained constant over the measurement time, and any temperature dependence was minimal due to the relatively short duration of the measurement tracks.
3) The nadir antenna noise temperature was assumed constant over the measurement track. It is reasonable to assume that the sea surface temperature (SST) remained relatively constant over the flight track, resulting in negligible errors due to fluctuations in the antenna noise temperature in the measurements.
4) Effects of rain, SST and sea surface salinity (SSS) are believed to be negligible in this analysis due to the relatively long GPS wavelength of 19 cm, which traverses rain with minimal signal loss and the very weak sensitivity to SST and SSS of GPS reflections as described in more detail in [8].

It is important to note that this waveform calibration is inextricably linked to the GNSS-R power scattering in the Z–V model. This model assumes a normal distribution for L-band limited sea surface slopes. The latter means that the radio wavelength imposes a limitation on surface wave spectral components participating in the scattering process. Other models could be used in this analysis with different scattering process assumptions. Given that the Z–V model is almost universally used in the GPS remote sensing community, this seemed the best choice available.

The first step in the calibration process is to determine a reference noise floor value from the calibration waveform as

$$\mathrm{CN_{ref}} = \sum_{\mathrm{noisebins}} C_{\mathrm{ref}} \qquad (1)$$

where C_{ref} is the 2-s averaged reference/calibration waveform in counts. The noise floor was computed as the average of a total of 40 delay bins before the start of the signal peak. The peak of the averaged reference waveform (in counts) was found as

$$C_{\mathrm{ref}}^{\mathrm{peak}} = \max\left[C_{\mathrm{ref}}\right]. \qquad (2)$$

The reference waveform total instrument gain was calculated as

$$G_{\mathrm{ref}} = \frac{C_{\mathrm{ref}}^{\mathrm{peak}} - \mathrm{CN_{ref}}}{P_{\mathrm{ref}}^{\mathrm{peak}}} \qquad (3)$$

where $P_{\mathrm{ref}}^{\mathrm{peak}}$ is the peak power of the model waveform at the reference MSS value.

Subsequently, using the reference gain G_{ref} determined using the averaged reference waveform and the model peak power at
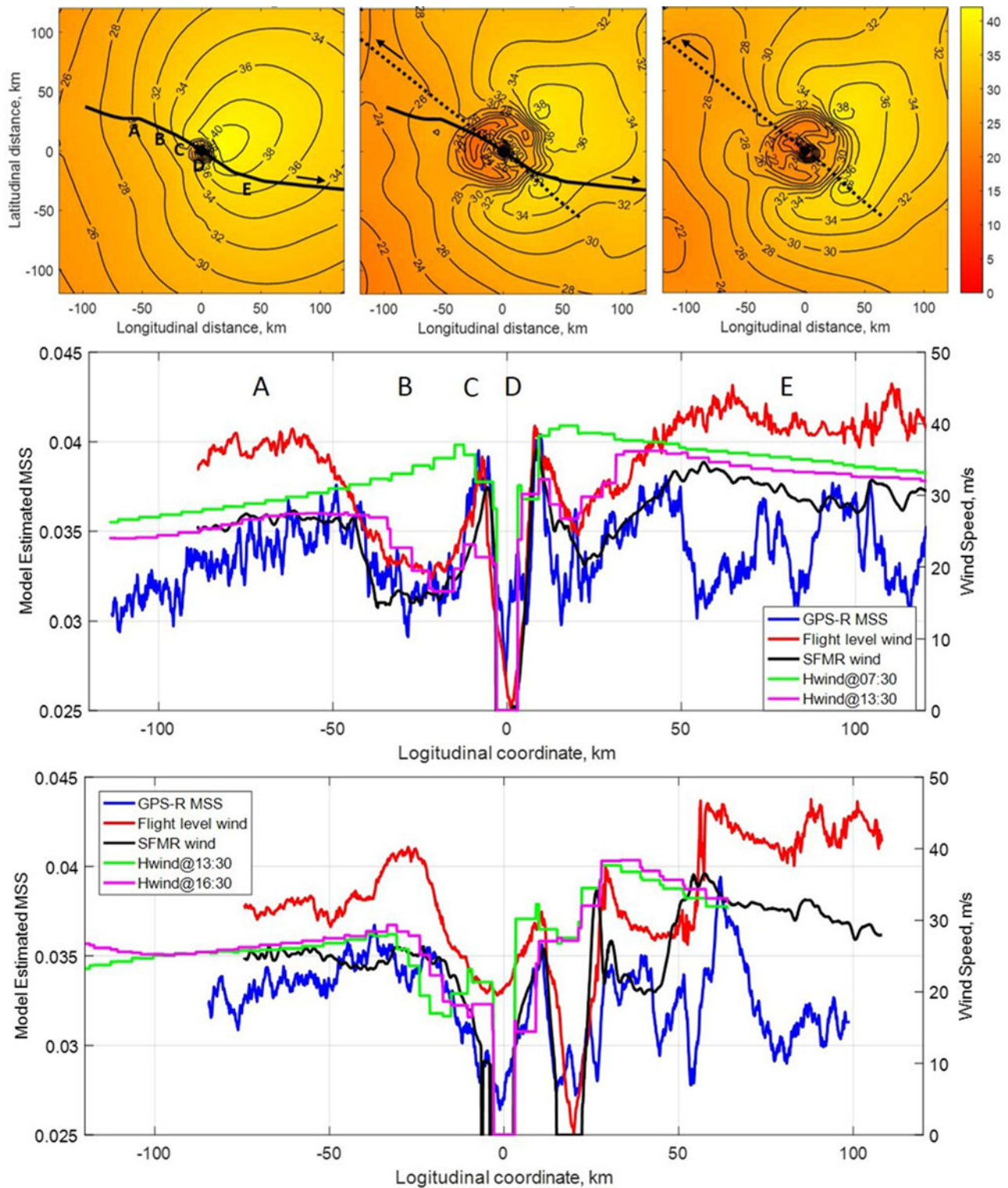
Fig. 5. Top panel shows maps of HWind estimated surface winds in Hurricane Ike at 7:30 (left), 13:30 (center), and 16:30 (right). Map coordinates are longitudinal and latitudinal distances in kilometer with respect to the center of the hurricane eye. Tracks 1 and 2 are shown by solid and dashed black lines, respectively. The arrows show flight direction of the aircraft. The calibration region within the HWind estimated wind fields is near region "A," for both tracks. Key features in the hurricane are indicated with letters and correspond to the MSS and wind estimates shown below in the middle panel (top). The hurricane eye is indicated by "D." The middle and bottom panels compare least squares estimated GPS-R MSS (blue) together with SFMR wind speed estimates (red), and HWind wind speeds (black) along the measurement tracks 1 (middle panel) and 2 (bottom panel) as a function of the longitudinal distance. The middle and bottom panels each have two HWind curves closest in time to the aircraft transit times. The middle panel letter markings correspond to the location of the aircraft over the hurricane as indicated in the top-left panel.

TABLE I
ESTIMATING WIND SPEED AND MSS FOR TRACK 1 CALIBRATION REFERENCE

Dropsonde Wind Estimated in Reference Region	28.0 m/s
10 Percent Error Lower Bound MSS Estimate at Reference	0.0288
Dropsonde Based MSS Estimate at Reference	0.0320
10 Percent Error Upper Bound MSS Estimate at Reference	0.0352

the reference MSS, scale all waveforms from counts to watts as

$$P_s = \frac{C - \mathrm{CN}}{G_{\mathrm{ref}}} \qquad (4)$$

where

$$\mathrm{CN} = \sum_{\mathrm{noisebins}} C \qquad (5)$$

and C represents the set of 1-s averaged delay waveform across the entire measurement track.

A. HWind Estimation of Surface Winds

A source of wind speed reference data during Hurricane Ike were the 6-h maps provided by [35] HWind product. These wind field maps are generated using multiple data sources and models.

The GPS-R measurements were collected around 10:24 (track 1) and 14:36 (track 2), whereas HWind maps were available at 7:30, 13:30, and 16:30. During that interval, Hurricane Ike was moving west-northwest at about 4 m/s. At 7:30, Hurricane Ike had a radius of maximum wind (RMW) of about 18 km. The hurricane wind field structure evolved significantly over the next 6 h. The RMW increased to about 48 km at 13:30, but the previous RMW was still evident as a local maxima. The structure changed little between 13:30 and 16:30. The 7:30 and 13:30 HWind maps are shown in Fig. 5 in a storm-relative reference frame with track 1 superimposed on both and track 2 superimposed on the 13:30 map as a dashed line.

B. Estimating Calibration Wind and MSS

The best available estimate of near-surface winds came from a dropsonde in the vicinity GPS-R collection track 1. The dropsonde indicated a mean wind speed below 500 m of 28 m/s in the calibration region less than 10 min before the start of GPS-R data collection in the same region. This wind speed was then converted to the reference MSS used in the waveform calibration using the [37] wind/wave model. The Elfouhaily et al. wave model accuracy is known to be worse at higher wind speeds. Therefore, it is expected to introduce an additional error in calibration MSS level. We attempt to bound the errors in our reference MSS by creating an uncertainty buffer, which allows us to quantify the biases in our MSS retrievals due to possible errors in the reference MSS value, while still allowing for meaningful comparison of wind and MSS correlation. Table I shows the range of reference MSS tested in order to bound the MSS retrieval errors. The dropsonde-based wind speed converted to MSS using the Elfouhaily et al. wave model was used as our best estimate.

The track 2 reference area was again in the same area (but at the end of the track) using the same dropsonde wind estimate, but a few hours later. HWind maps indicated that in this region away from the hurricane eye and strong wind bands, the wind speeds remained relatively stable over the 6-h interval between available HWind maps. Unfortunately, additional dropsondes wind estimates were not available in this region.

IV. MSS ESTIMATION USING GPS-R MODEL

The general procedure for converting the calibrated GPS reflection waveforms to estimates of MSS consists of performing a least squares model fit of the complete series of calibrated waveforms over each measurement track using modeled waveforms generated with the Z–V model.

The detailed steps in the estimation technique include the following.

1) Determine the bistatic reflection geometry using GPS ephemeris from [38] (IGS), the aircraft position log (determined by an GPS navigation receiver), and the surface specular reflection location calculated as in [7].

2) Input the complete reflection geometry into the GPS-R Z–V model and generate a series of nonnormalized delay waveforms over the complete measurement track. Generate model waveforms using the dynamic transmitter/receiver geometry at every measurement time epoch over a full range of surface MSS values.

3) Calibrate the CUBR GPS-R waveforms from counts to watts using the method described in Section III. The resulting waveforms are now in units of watts, referenced to the MSS value derived from the dropsonde wind speed estimate and the Elfouhaily et al. wave model.

4) Perform a least squares cost function fit for each calibrated measurement from the CUBR instrument waveforms over two dimensions: 1) delay bin alignment (i.e., slide model waveform back and forth in delay to achieve best peak delay bin match) and 2) full range of MSS.

The above steps result in a GPS-R model estimate of the MSS values for each calibrated delay waveform along the flight track for each of the two reflection tracks obtained simultaneously from two satellites. The MSS estimates for two simultaneous reflection tracks were averaged together to produce a single MSS estimate along the flight tracks. Finally, the MSS estimates for each flight track were averaged using a 10-s running window average. These MSSs are shown in blue in Fig. 5 (two bottom panels). The MSS retrieval results for both satellites, for both flight tracks, were relatively similar with few significant diversions in MSS between them. We believe that averaging the two satellite MSS estimates along each track provides a better indication of the actual surface MSS in the vicinity of the aircraft ground tracks.

A. GPS-R MSS Estimation Results

The GPS-R MSS estimated during track 1 as compared with the aircraft flight level winds, SFMR estimated surface winds, and Hwind wind estimates is shown in Fig. 5.

Area "A," represents the start of track 1, where the GPS-R MSS estimate, the HWind winds, and SFMR winds all show a gradual increase as the reflection approached the eye. At this point, Hurricane Ike was in an interesting state of having what seemed to be a "double" eye, which very likely could have been due to an eye wall replacement cycle. Over area "B," a region where the MSS and winds noticeably decrease is clear from the GPS-R MSS (blue) and SFMR winds (black) traces. The HWind wind fields (green trace) dip more moderately over this interval. At point "C," all three values show a clear increase, as this "inner eye" is detected.

The eye of the hurricane is marked as "D" and all three estimates drop off accordingly, although the GPS-R MSS estimate is slightly higher than the SFMR and HWind estimates. The GPS reflected signal due to nature of the forward quasi-specular scattering mechanism is more affected by the sea state than that of the SFMR. The sea state in the hurricane eye is determined by relatively long waves arriving from areas with a higher wind speed (fresh swell). Since the SFMR sensing mechanism is based on a foam coverage produced by much shorter waves due to local wind, the SFMR wind estimate is less sensitive to the sea state than the GPS-R MSS estimate.

There is less agreement over the area labeled "E," where the GPS-R MSS sometimes shows a negative bias with respect to the SFMR. This could be a result of short-fetched (young) seas characterized by a relatively smaller MSS compared to that of the developed seas. The GPS-R measurements showed almost a cyclical fluctuation of MSS over this interval, as did the SFMR wind speed estimates (albeit out of sync with the fluctuations of the GPS-R MSS changes). The HWind wind estimates showed a more uniform wind speed decrease over this interval. As will be shown in the following, the MSS and SFMR wind were well correlated up until about 10:55 UTC, and negatively correlated over much of area "E," with regard to the MSS disagreement with SFMR wind trends in region "E." The changes in the aircraft flight level winds (red trace) generally correspond with the SFMR winds, with the flight level winds being generally higher as would be expected.

B. Approximating the GPS-R MSS Retrieval Uncertainty

The GPS dropsonde in the vicinity of the calibration regions provided a reasonable estimate of the wind speed in the calibration regions of the hurricane. However, it is still believed that there could be significant error in our reference estimates of wind and MSS, which will bias the resulting GPS-R MSS retrievals.

These error factors include the following:
1) the inherent noisy measurements of the dropsonde as it approached the surface and the averaging of the wind speeds below 500 m;
2) the high temporal and spatial variation of the winds in a hurricane will result in temporal and spatial colocation errors; and
3) using the Elfouhaily *et al.* wave model to convert from wind to MSS in a hurricane (even relatively removed from the intense storm region, and at wind speeds below 30 m/s) is risky.
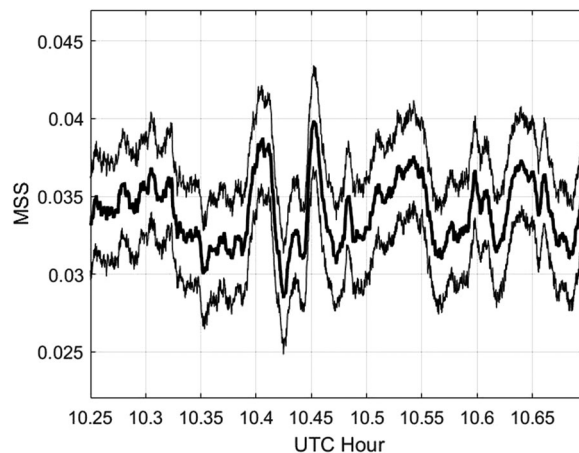

Fig. 6. Estimated GPS-R MSS at the best estimate reference wind and MSS (thick curve), as well as the estimates obtained using the 10% low and high MSS calibration reference values (above and below curves).

However, the only other wind to MSS model validated in hurricanes is the Katzberg *et al.* model, which we prefer not to use in order to keep our results independent from the Katzberg model to provide a more useful comparison.

In order for us to attempt to bound the errors in the GPS-R MSS estimation due to these two factors, we have added a 10% error buffer below and above the best estimated MSS in the calibration region. This will provide a reasonable high/low bound of our GPS-R results. As the primary purpose of this research is to explore the correlation between wind and waves, errors in the absolute level of the GPS-R MSS estimation will not be affected by a shift up or down in the MSS average magnitude (where the MSS and wind fluctuations drive the correlation). The range of values tested for our reference MSS is listed in Table I. How these values impact the GPS-R MSS retrievals is shown in Fig. 6. All three curves in this figure were generated using a 10-s running window average applied to the raw MSS data.

Note that the width and integral GPS-R MSS retrievals performed below are not affected by these errors (these retrievals are based solely on the reflected waveform shape). However, these retrievals tend to slightly underestimate the MSS when compared to the least squares method.

V. CORRELATION OF WIND AND MSS OVER MEASUREMENT TRACKS

For well-developed seas formed under uniform wind conditions, it is natural to expect the wave propagation direction to be the same as the wind direction. In this case, the wave field has a unimodal structure, and for winds between 2 and 24 m/s, it can be satisfactorily described by the Elfouhaily *et al.* directional wave spectrum [37], or by other similar models. However, this is not what happens in hurricanes where wind speed is quickly changing radially and wind direction is rotating counter clockwise around the eye. The forward motion of the hurricane further complicates the situation, so the dominant wave direction and the local wind vector in hurricanes are frequently not aligned, and the dominant waves can propagate up to 90°

from the downwind direction, or even in the opposite direction [39]–[45]. Behind the eye, the wave field can even be trimodal [39].

The behavior of surface waves in hurricane conditions has been reproduced in the numerical models [42]–[44]. Along these lines, it has been shown in [14] and [46] that different segments of a hurricane can differ significantly with respect to surface waves, notably swell. The fact that dominant wave direction and the wind vector in hurricanes are mostly misaligned leads to a wave development under short fetch conditions.

The physical processes behind those observable features of the hurricane wave field are complex and numerous (see, e.g., [2], [3], [13], [14], [42], [43], [45], [47]). In wave numerical models, the wave field behavior is formulated in terms of the spectrum of elevation variance E being a function of wavenumber $\overrightarrow{\kappa}$. According to [2], there are 11 identifiable physical processes that have a first-order effect on $E(\overrightarrow{\kappa})$. They include wind input, wave breaking, wave–wave, wave-current and nonlinear interactions and evolution, and wave breaking dissipation by turbulence and viscosity.

Significant efforts are made by oceanographers to monitor those processes by performing measurements *in situ* or with remote sensing tools. Altimeters are capable to measure such sea-state parameters as the sea surface elevation variance σ_{η}^{2} (or an SWH, which is equal to $4\sigma_{\eta}$), and an MSS

$$\sigma_{\eta}^{2} = 4 \int_{0}^{k_{*}} E(\overrightarrow{\kappa}) d^{2}\kappa \qquad (6)$$

$$\mathrm{MSS} = \int_{0}^{k_{*}} \kappa^{2} E(\overrightarrow{\kappa}) d^{2}\kappa. \qquad (7)$$

Due to different signal carrier frequencies, the cutoff wavenumbers k_{*} are different for altimeters and L-band GPS reflectometers. Because of an insufficient bandwidth of the probing signal, the L-band GPS reflectometers can measure only the L-band limited MSS.

In the following, we attempt to demonstrate the correlation between surface GPS-R MSS estimates and near-surface wind speeds. The reference wind speeds used in this analysis are the surface wind speeds estimated by SFMR using C-band surface brightness temperatures as described in [27]. In the case of comparing GPS-R estimated MSS and SFMR winds, it should be noted that the measurements are not exactly colocated. It is often the case that up to several kilometers of distance to exist between the spatial locations of the two wind estimates.

The top panel in Fig. 7 shows the track 1 results for GPS-R MSS estimated averaged over a 10-s running window and flight level and SFMR wind speeds. This panel shows the same GPS-R MSS estimates as Fig. 5 except that the data are presented as a function of a flight time.

Additionally, three new areas are labeled: Area "A" is a small region at the beginning of the track, which showed weak correlation between MSS and wind; Area "B," which showed strong correlation between MSS and wind; and Area "C," which showed negative correlation between MSS and wind.

There is some correlation between the SFMR estimated wind fields and the GPS-R estimated MSS fluctuations in Area "B."
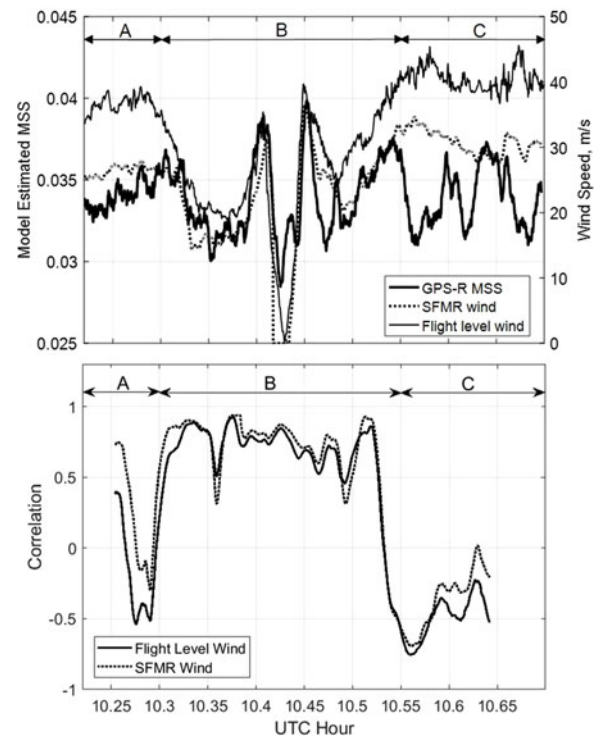

Fig. 7. (Top) Averaged GPS-R MSS estimates and corresponding SFMR and flight level wind speed estimates over track 1. (Bottom) Correlation between GPS-R MSS and SFMR wind (solid curve) and flight level wind (dotted curve) along track 1. Labels corresponding to the top panel.

TABLE II
CORRELATION BETWEEN THE GPS-R MSS ESTIMATES AND SFMR AND
FLIGHT LEVEL WINDS OVER THE FIVE LABELED REGIONS DURING THE
HURRICANE EYE TRANSECT OF TRACK 1

Region	GPS-R/SFMR	GPS-R/Flight Level Wind
A	0.38	0.24
B	0.85	0.92
C	0.79	0.84
D	0.90	0.88
E	-0.32	-0.12

In order to quantify this correlation, the GPS-R MSS estimates and the SFMR wind speeds were correlated over a running 4-min window. Different correlation durations result in slightly different correlation results across the track. However, we found that a using a 4-min window provides a reasonable duration, which mitigates noise effects and is not too long so as to be effected by the hurricane wind spatial variation. These results are shown in the bottom panel of Fig. 7.

With only a couple of brief exceptions at the beginning of the track, the flight level and SFMR wind speeds and the GPS-R MSS estimates correlate to greater than 0.7 up until slightly before UTC hour 10:55. After this point, the correlation abruptly shifts negative as is also apparent in the bottom panel of Fig. 7 as the MSS and SFMR winds start moving in opposite directions. Mean correlation values from the bottom panel of Fig. 7 are shown for clarity in Table II.

A similar pattern was observed in the track 2 GPS-R MSS and SFMR wind speed measurements. Refer to the top panel of Fig. 8 for the GPS-R MSS retrievals and the SFMR wind
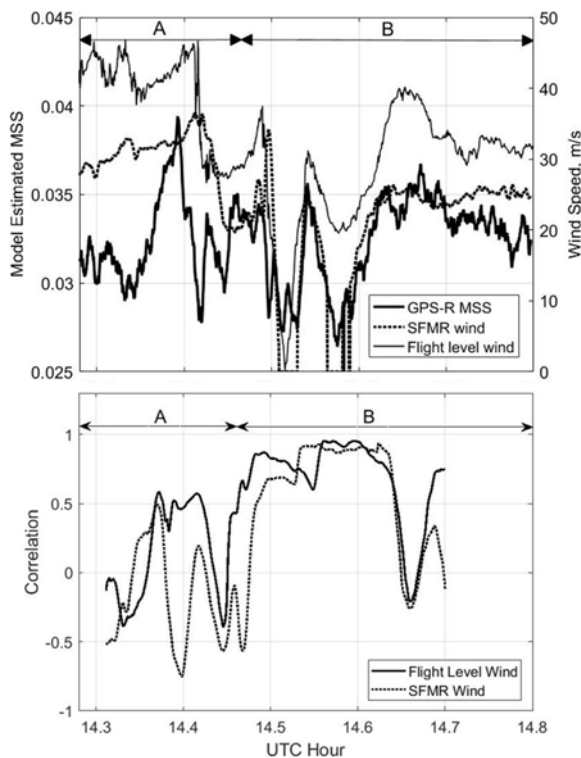
Fig. 8. (Top) Averaged GPS-R MSS estimates and corresponding SFMR and flight level wind speed estimates over track 2. (Bottom) Correlation between GPS-R MSS and SFMR wind (solid curve) and flight level wind (dotted curve) along track 2. Labels corresponding to the top panel.

estimates and to the bottom panel of the same figure for the results of the 4-min running correlation window of MSS and wind over the duration of track 2.

Hurricane Ike was moving 4 m/s toward the west-northwest. Track 1 was approximately along the path of Hurricane Ike, but flying in the opposite direction. Track 2 traversed the hurricane from roughly the southeast to the northwest (see Fig. 1). In the top panel of Fig. 8 the region marked Area "A" is at the beginning of track 2 (the back side of the hurricane), and Area "B" is at the end of the track (front side of the hurricane). In this case, the back side of the hurricane (Area "A") shows weaker correlation between MSS and wind, whereas the front side of the storm (Area "B") shows areas of stronger correlation of the GPS-R MSS estimates and SFMR wind speeds.

Would the peculiarities of MSS behavior in Hurricane Ike be expected in observations of every hurricane? Similar variations in the hurricane wave structure in the various regions of the storm are routinely observed. Hurricane Ike had been very uniform in intensity, track, and forward speed for 16 h prior the GPS-R observations [48]. The WSRA directional wave spectra indicated that in front of the hurricane, there was an azimuthally narrow unimodal wave system of about 300–350 m wavelength. Behind the storm, the wave system was multimodal with a half-power width of about 90° and wavelengths of 150–200 m. That situation is typical and might have caused the asymmetry. However, during this flight, the back side of Hurricane Ike was in the area of the loop current [49]. The interaction between the

wave field and the loop current might also have produced the observed asymmetry. Observations in a uniform ocean environment would be needed to resolve this issue. The hypothesis we propose above does not explain the data behavior at every point over the two tracks, it is only meant to start a discussion and provide a partial explanation to a very complicated problem.

VI. MSS ESTIMATION RESULTS USING OTHER OBSERVABLES

In Section V, we presented least squares fitting MSS estimation results based on fitting the measured waveforms with the modeled waveforms. This method has its own limitations and drawbacks. Notably, it is sensitive to noisy regions of the measured waveform such as the trailing edge that may lead to biases, and it is time-consuming. Because we would like to exclude not well determined power, gain, and geometry factors from a consideration, we implemented a special calibration procedure described in Section III. To perform the calibration, we use the dropsonde wind speed as an input for the Elfouhaily *et al.* wave model to estimate the MSS in the calibration region. Of course, use of the Elfouhaily *et al.* wave model at winds above 24 m/s in a vicinity of the hurricane is risky (albeit made out of necessity), which adds some uncertainty to this procedure.

We tried other approaches that are less sensitive to the behavior of the waveform trailing edge, are not dependent on fluctuations in the waveform peak, and do not require the above-mentioned calibration procedure. Also, they are less time-consuming than the waveform fitting method because they rely on much simpler characteristics of the waveform, such as a shape. Two additional observables have been considered: the integral of the normalized (by the peak power) waveform along the delay axis and the width of such a waveform at the 0.5 level. An observable, very similar to the waveform integral but instead employing full delay-Doppler maps, was proposed and used for airborne GNSS-R wind retrievals in [34].

To retrieve the MSS from those observables, we created two lookup tables of the modeled normalized waveforms for a range of receiver heights, the angles of incidence, and the MSS input values using the Z-V theoretical model. From them, we generated corresponding lookup tables for integrals and widths. The time series of the integrals and widths of the measured normalized waveforms were also calculated for every second. After that, we performed matching between the experimental values and modeled values from the lookup tables. As a result of this matching, we retrieve the MSS for each of the two GPS satellites along first and second track.

Fig. 9 represent the MSS retrieval results for both tracks using the waveform integral and width compared against the MSS obtained with the least squares method. In both the cases, the MSS estimates from both PRNs have been averaged together.

Fig. 9 demonstrates most of the time a good correlation between MSS curves for all three methods. A number of peaks and minima that correspond to various features of hurricane are reproduced by all three curves for both tracks 1 and 2. In terms of the MSS absolute level, a better correspondence between all curves is observed for track 2 (bottom panel on Fig. 9). The result for track 1 (top panel) is that the estimates of MSS using the
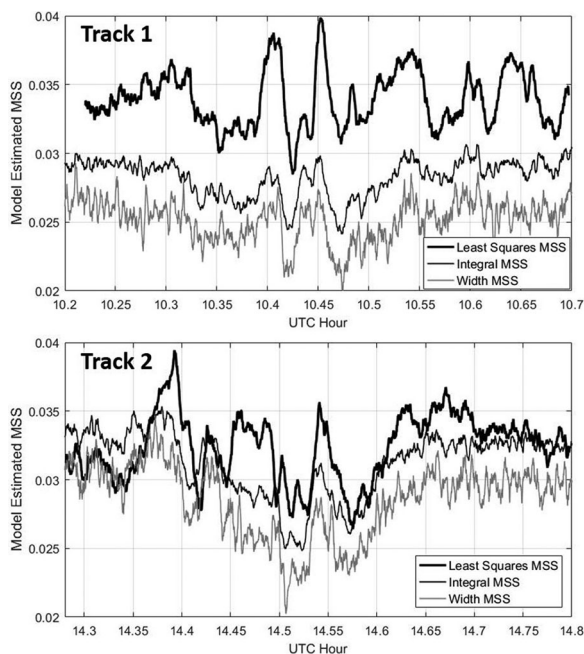
Fig. 9. Comparison of estimated MSS using the least squares method, the integral and width of the GNSS-R waveform for track 1 (top) and track 2 (bottom). MSS here is an average of MSS obtained from two satellites (PRNs).
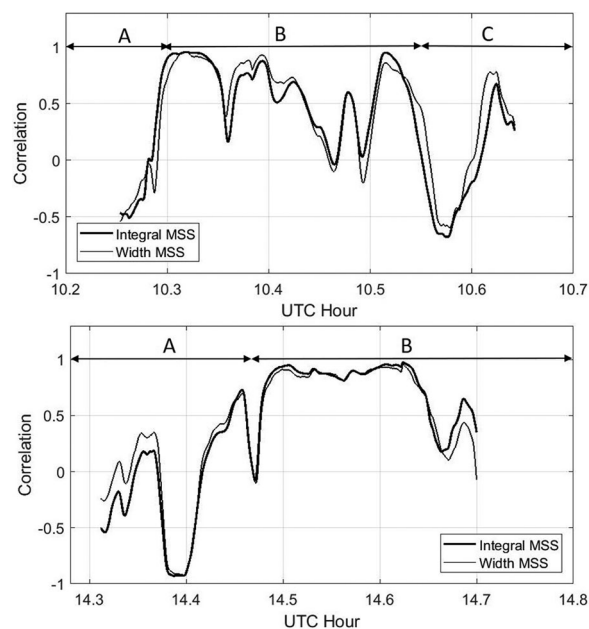

Fig. 10. Correlation of GPS-R integral and width estimated MSS values with SFMR wind speed for track 1 (top) and track 2 (bottom). Notations A–C for various areas have the same meaning as in Figs. 7 and 8.

integral method is lower than the least squares MSS by roughly 15%–20%. For the width MSS, the bias reaches 25%. There are concerns that the value of the least squares MSS might be overestimated. This could be explained by a number of factors including the following:

1) an error in the calibration reference wind resulting in a positive bias to the least squares MSS values;
2) an unaccounted-for correction (such as for the receiver antenna gain), which would bias the least squares MSS retrievals more than a retrieval based on the waveform width or integral; and
3) a limitation of the Elfouhaily *et al.* wave model, which is based on nonhurricane air–sea interaction data.

Given some of the unknowns in the experiment setup, both of the above errors could exist to some degree; however, it is not possible to prove given the limited knowledge in some areas of the experiment configuration.

The normalization of the waveforms by the peak power used in the retrievals based on the waveform integral or width eliminates the influence of listed above factors. That makes us think that these methods should work better than the least squares method. However, the issue of systematic bias of order of 10% between the integral MSS and the width MSS needs to be resolved. The explanation of this difference could be that the probability of wave slopes in hurricanes does not exactly follow the Gaussian distribution (the assumption made in the Z-V scattering model). Such parameters of the non-Gaussian slope statistics as kurtosis and peakedness might be as important as the MSS. Therefore, the GPS reflected waveform shape could depart from the one expected for the case of Gaussian slope statistics. In this case, the waveform integral and width are ceased to be functions only of the MSS. That could lead to observed differences between integral- and width-based MSS retrievals. More likely, the reason for a less noisy integral-based MSS retrieval compared to the width-based MSS retrieval is the fluctuations of the waveform shape are averaging while the integration over delay bins is performed, whereas the width of the waveform remains affected by these fluctuations. In a sense, it is equivalent to using a larger surface footprint (with a stronger averaging) in the former case.

To summarize the discussion of the differences and similarities of the MSS retrievals using all three approaches, we should say that at this point we cannot say for certain which one is best as we do not have a solid MSS truth reference to compare to.

An analysis of the correlation between the width and integral estimated MSS values and the SFMR wind speeds along both tracks is shown in Fig. 10. The figures show that the correlation over area "B" in track 1 is weaker than for the least squares estimated MSS, whereas the higher correlation over area "B" in track 2 is still evident.

VII. COMPARISON OF WSRA AND GPS-R MSS WITH SFMR WIND SPEED

The WSRA provides estimates of the MSS of the ocean surface by using the Ku-band radar backscattered power falloff with incidence angle [29]. The WSRA MSS originates from the wave spectra limited by the high frequency cutoff corresponding to the Ku-band frequency, whereas the similar cutoff for the GPS-R MSS is dictated by much lower, L-band frequency. WSRA MSS estimates for track 1 are plotted together with SFMR wind estimates on the top panel of Fig. 11. Similar to the GPS-R MSS estimates, the fluctuations of the WSRA MSS tend to correspond better to the SFMR winds on the western side of the hurricane. During the 2008 hurricane season, the WSRA
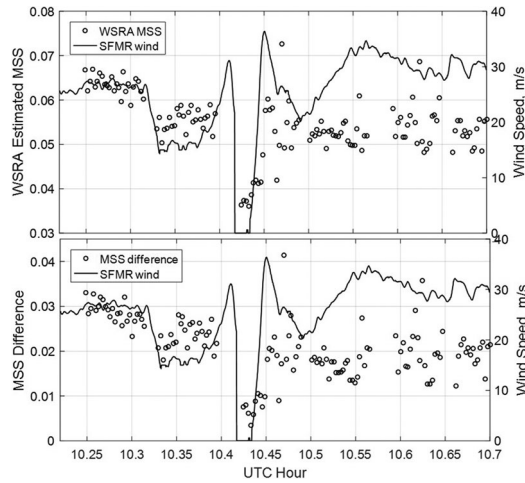
Fig. 11. (Top) WSRA MSS (circles) and SFMR wind speed (solid curve) over the first aircraft measurement track (track 1). (Bottom) Difference between Ku-band WSRA MSS and L-band GPS-R MSS for the same track (circles). SFMR wind speeds estimates included for comparison.

Fig. 12. Ratio between Ku-band WSRA MSS and three different L-band GPS-R MSS estimates for track 1 (circles).

was configured to record only raw I&Q data. This was done to provide a valuable dataset for postflight work on optimization of the WSRA real-time processing algorithm. Throughout the Ike flight, many of the radar parameters were varied by the on-board operator, causing WSRA data gaps. As a result, the WSRA data records were not sufficiently continuous to perform a correlation analysis with SFMR winds along either track.

The difference between the WSRA and GPS-R estimates of MSS provides useful information on how the measurement frequency influences the estimation. The 16-GHz WSRA and the 1.57-GHz GPS-R are observing different portions of the wave spectrum $S(\overrightarrow{\kappa})$. The higher frequency measurement is sensing higher MSS in the shorter waves. The difference ΔMSS between the WSRA and GPS-R MSS estimates gives the short-wave portion of slope variance between the GPS-R and WSRA cutoff wavenumbers, k_{GPS-R} to k_{WSRA} [see (6) and (7)]

$$\Delta\text{MSS} = \int_{k_{GPS-R}}^{k_{WSRA}} \kappa^2 E(\overrightarrow{\kappa}) d^2\kappa. \tag{8}$$

A similar result was shown in [5] where the difference between the MSS obtained with the laser altimeter and the Ka-band radar altimeter was calculated to obtain information on the short gravity and gravity-capillary wave contributions. In our case, these contributions come from somewhat longer surface waves.

The difference between the MSS estimates from WSRA and GPS-R is shown on the bottom panel of Fig. 11. Here, we use the least square estimates for the GPS-R MSS. The WSRA MSS is systematically higher than the GPS-R MSS. However, the degree of correlation is high because a significant portion of the MSS value for both the WSRA and GPS-R originates from the integral of the slope spectrum over the same wavenumbers, zero to the GPS-R cutoff wavenumber. The low-frequency part of the slope spectrum and its peak position are functions of wind speed (and other parameters such as wave age, incoming fresh swell, etc.). Therefore, the common part of the MSS for both
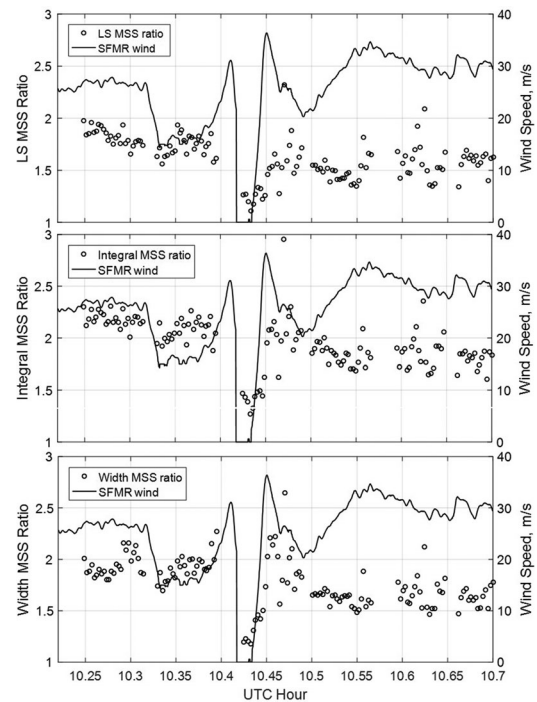
cases depends on wind speed and other parameters, ensuring correlation between MSS obtained with the different techniques.

Decorrelation and variable offset between the MSS values comes from the integral over the wavenumber interval between the WSRA and the GPS-R high-frequency cutoffs. Since we do not know the exact expression for that part of the slope spectrum (its dependence on wind speed and other parameters), we cannot calculate the corresponding MSS offset.

An additional assessment of the GPS-R MSS estimates using waveform least squares, integral and width observables was performed by calculating the ratio between the WSRA and GPS-R MSS estimates using all three methods. The comparison is shown in Fig. 12. The modeling of the WSRA and GPS-R MSS as a function of wind speed using the Elfouhaily et al. wave spectrum predicts a WSRA to GPS-R MSS ratio near 2 for winds above 20 m/s. Fig. 12 shows that the WSRA to integral MSS ratio (the medium panel) exhibits a better agreement with the modeling results: closer to the value of 2 and less scatter comparing with two other cases.

VIII. GENERATION OF GPS-R MSS TO SFMR WIND SPEED FUNCTION FOR HURRICANE IKE

The sensitivity of GPS-R estimated MSS at high wind speeds and in hurricanes is of critical importance to NASA missions like CYGNSS and possibly follow on missions. It has been clearly demonstrated in [25] that GPS reflections remain sensitive to changes in wind and MSS in hurricanes at very high winds speeds. This research is meant to provide an additional validation of these previous experiments, including the generation of
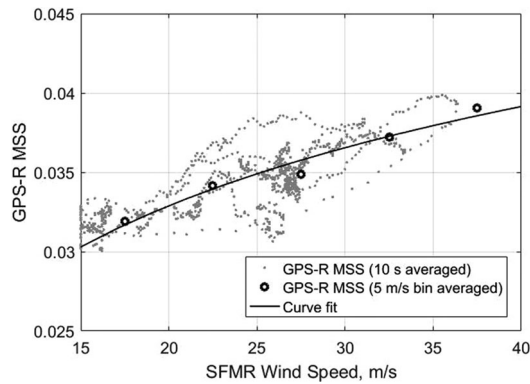
Fig. 13.   Plot of GPS-R MSS estimates versus SFMR wind speeds over the regions of high wind/wave correlation during track 1. Gray dots are MSS averaged using a 10-s boxcar filter. Circles are the averaged MSS values in 5 m/s wind speed bins. Black line represents a natural logarithmic curve fit to the averaged MSS bins.

a new wind speed (as estimated by SFMR) to MSS relationship linked solidly to the established GPS-R Z–V model.

In this regard, this CUBR instrument collected a limited, but we believe sufficient number of measurements between winds of 15 and 40 m/s to provide a useful (although not definitive) MSS to wind reference function in this range, which demonstrates the MSS versus wind sensitivity at high wind speeds. A total of 4000 measurements from both tracks 1 and 2 over wind speeds from 15 to 40 m/s were used to calculate an MSS to wind relationship. Only data with MSS/wind correlation greater than 0.5 were used to generate the relationship.

These limited number of MSS/wind points from this single aircraft flight results in a slightly underdetermined estimation problem. However, the data do show a clear wind/wave trend, which we believe is useful for comparison with existing models.

Fig. 13 shows all of the GPS-R MSS and SFMR wind estimates along the measurement track, with the GPS-R MSS averaged using a 10-s boxcar filter. The upward trend in MSS estimates is clearly visible even at 35 m/s. This datum was then fit to a logarithmic function to generate a surface wind speed to MSS function to estimate the high wind sensitivity of GPS reflections. A logarithmic function was chosen as it is most consistent with the existing Katzberg and Elfouhaly wind/wave models and generally captures the expected behavior of the wind/wave relationship (including at high wind speeds). The relationship between winds and MSS was found to fit the following function:

$$\text{MSS} = a + b \ln U_{10}. \tag{9}$$

A search for the best natural logarithmic fit to the data points resulted in a wind wave relationship of the form shown in (9), with $a = 0.0058489$ and $b = 0.0090269$, where U_{10} is the near-surface wind speed over the range of between 15 and 40 m/s.

A. Comparisons of L-Band Wind Speed to MSS Relationship With Existing Models

The relationship between high winds and MSS at L-band has long been an open question in GPS remote sensing. The initial
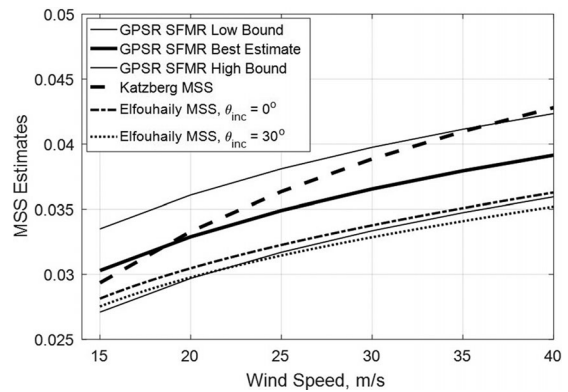

Fig. 14.   Plot wind to wave relationships for GPS-R/SFMR results versus multistorm results from [15] and the wind to MSS model [37]. High and low thinner black lines mark the 10% error lower and upper bounds from Table I.

TABLE III
COMPARISON OF MSS AS A FUNCTION OF WIND SPEED AS CALCULATED BY (9) USING GPS-R MSS AND SFMR, MSS PREDICTIONS FROM [15] AND THE WIND TO MSS MODEL [37]

Wind Speed	Eq.(9) MSS	Katzberg MSS	Elfouhaily MSS
15 m/s	0.0291	0.0294	0.0272
20 m/s	0.0317	0.0333	0.0294
25 m/s	0.0337	0.0364	0.0311
30 m/s	0.0354	0.0389	0.0325
35 m/s	0.0368	0.0410	0.0338
40 m/s	0.0380	0.0428	0.0349

results from aircraft experiments showed that the semiempirical model of Elfouhaily *et al.* provided reasonable results at lower wind speeds (up to about 20 m/s). However, the experiments performing wind speed retrievals in hurricanes were shown to have more sensitivity at higher wind speeds than predicted by the Elfouhaily *et al.* wave model. Katzberg *et al.* used data from the NASA Langley receiver over several hurricanes to derive an empirical wave to wind model over a larger range of wind speeds. How the wind wave relationship derived above compares to these models over a range of wind speeds between approximately 15 and 40 m/s is shown in Fig. 14. Table III shows the predicted MSS values for a range of wind speeds as calculated using (9).

IX. Summary

This paper has shown a detailed analysis of several GPS-R MSS measurements techniques across two eye transects of Hurricane Ike in 2008, and demonstrated areas of strong and weak wind/wave correlation near and outside the hurricane eye. The finer processing possible with the raw IF sampled data allowed for a detailed comparison of MSS and wind speed fluctuations across the dramatically changing conditions in the hurricane environment. It was found that, for these two tracks, the area ahead of the hurricane eye showed stronger correlation between the GPS-R MSS and the flight level and SFMR wind speeds than the area behind it. An empirical relationship between GPS-R estimated MSS and SFMR wind speed was derived over the full range of wind speeds present in the hurricane.

We can conclude that forward scattered L-band GPS signals generally can be used to monitor hurricane winds with a speed up

to 40 m/s, but the GPS-R measured MSS values may not always correlate well with wind speeds in some areas of a hurricane.

REFERENCES

[1] N. M. Frew *et al.*, "Air-sea gas transfer: Its dependence on wind stress, small-scale roughness, and surface films," *J. Geophys. Res.—Oceans*, vol. 109, 2004, Art. no. C08S17, doi: 10.1029/2003JC002131.

[2] M. A. Donelan, M. Curcic, S. S. Chen, and A. K. Magnusson, "Modeling waves and wind stress," *J. Geophys. Res.*, vol. 117, 2012, Art. no. C00J23, doi: 10.1029/2011JC007787.

[3] B. G. Reichl, T. Hara, and I. Ginis, "Sea state dependence of the wind stress over the ocean under hurricane winds," *J. Geophys. Res.—Oceans*, vol. 119, no. 1, pp. 30–51, 2014.

[4] E. J. Walsh *et al.*, "Measuring sea surface mean square slope with a 36-GHz scanning radar altimeter," *J. Geophys. Res.*, vol. 103, pp. 12587–12601, 1998.

[5] D. Vandemark, B. Chapron, J. Sun, G. H. Crescenti, and H. C. Graber, "Ocean wave slope observations using radar backscatter and laser altimeters," *J. Phys. Oceanogr.*, vol. 34, pp. 2825–2842, 2004.

[6] S. Gleason, "Remote sensing of ocean, ice and land surfaces using bistatically scattered GNSS signals from low earth orbit," Ph.D. dissertation, Univ. Surrey, Guildford, U.K., 2006.

[7] S. Gleason, S. Lowe, and V. Zavorotny, "GNSS applications and methods," in *Remote Sensing With Bistatic GNSS Reflections*, S. Gleason and D. Gebre-Egziabher, Eds. Norwood, MA, USA: Artech House, 2009, pp. 399–436.

[8] V. Zavorotny, S. Gleason, E. Cardellach, and A. Camps, "Tutorial on remote sensing using GNSS bistatic radar of opportunity," *IEEE Geosci. Remote Sens. Mag.*, vol. 2, no. 4, pp. 8–45, Dec. 2014.

[9] C. Ruf *et al.*, "New ocean winds satellite mission to probe hurricanes and tropical convection," *Bull. Amer. Meteorol. Soc.*, vol. 97, pp. 385–395, 2016, doi: 10.1175/BAMS-D-14-00218.1.

[10] C. Ruf *et al.*, *CYGNSS Handbook*. Ann Arbor, MI, USA: Univ. Michigan Press, 2014.

[11] S. Gleason, "Space based GNSS scatterometry: Ocean wind sensing using empirically calibrated model," *IEEE Trans. Geosci. Remote Sens.*, vol. 51, no. 9, pp. 4853–4863, Sep. 2013.

[12] M. P. Clarizia and C. S. Ruf, "Wind speed retrieval algorithm for the cyclone global navigation satellite system (CYGNSS) mission," *IEEE Trans. Geosci. Remote Sens.*, vol. 54, no. 8, pp. 4419–4432, Aug. 2016.

[13] S. S. Chen, J. F. Price, W. Zhao, M. A. Donelan, and E. J. Walsh, "The CBLAST-hurricane program and the next-generation fully coupled atmosphere-wave-ocean models for hurricane research and prediction," *Bull. Amer. Meteorol. Soc.*, vol. 88, no. 3, pp. 311–374, 2007.

[14] L. H. Holthuijsen, M. D. Powell, and J. D. Pietrzak, "Wind and waves in extreme hurricanes," *J. Geophys. Res.*, vol. 117, pp. 1–15, 2012, Art. no. C09003, doi: 10.1029/2012JC007983.

[15] S. J. Katzberg, O. Torres, and G. Ganoe, "Calibration of reflected GPS for tropical storm wind speed retrievals," *Geophys. Res. Lett.*, vol. 33, no. 18, pp. 1–5, 2006, Art. no. L18602, doi: 10.1029/2006GL026825.

[16] C. Hall and R. Cordy, "Multistatic scatterometry," in *Proc. IEEE Int. Geosci. Remote Sens. Symp.*, Edinburgh, U.K., 1988, pp. 561–562.

[17] M. Martin-Neira, "A passive reflectometry and interferometry system (PARIS): Application to ocean altimetry," *ESA J.*, vol. 17, pp. 331–355, 1993.

[18] J. L. Garrison, S. J. Katzberg, and M. I. Hill, "Effect of sea roughness on bistatically scattered range coded signals from the global positioning system," *Geophys. Res. Lett.*, vol. 25, no. 13, pp. 2257–2260, Jul. 1998.

[19] A. Komjathy, V. U. Zavorotny, P. Axelrad, G. H. Born, and J. L. Garrison, "GPS signal scattering from sea surface: Wind speed retrieval using experimental data and theoretical model," *Remote Sens. Environ.*, vol. 73, pp. 162–174, 2000.

[20] M. Armatys, "Estimation of sea surface winds using reflected GPS signals," Ph.D. dissertation, Univ. Colorado Boulder, Boulder, CO, USA, 2001.

[21] E. Cardellach, G. Ruffini, D. Pino, A. Rius, A. Komjathy, and J. Garrison, "Mediterranean balloon experiment: Ocean wind speed sensing from the stratosphere using GPS reflections," *Remote Sens. Environ.*, vol. 88, no. 3, pp. 351–362, 2003.

[22] O. Germain, G. Ruffini, F. Soulat, M. Caparrini, and P. Silvestrin, "The eddy experiment II: GNSS-R speculometry for directional sea roughness retrieval from low aircraft," *Geophys. Res. Lett.*, vol. 31, no. 21, pp. 1–4, 2003, Art. no. L21307, doi: 10.1029/2004GL020991.

[23] F. Soulat, "Sea surface remote sensing with GNSS and sunlight reflections," Ph.D. dissertation, Universitat Politecnica de Catalunya, Barcelona, Spain, 2004.

[24] S. J. Katzberg, R. A. Walker, J. H. Roles, T. Lynch, and P. G. Black, "First GPS signals reflected from the interior of a tropical storm: Preliminary results from hurricane Michael," *Geophys. Res. Lett.*, vol. 28, pp. 1981–1984, 2001.

[25] S. J. Katzberg and J. Dunion, "Comparison of reflected GPS wind speed retrievals with dropsondes in tropical cyclones," *Geophys. Res. Lett.*, vol. 36, 2009, Art. no. L17602, doi: 10.1029/2009GL039512.

[26] S. J. Katzberg, J. Dunion, and G. G. Ganoe, "The use of reflected GPS signals to retrieve ocean surface wind speeds in tropical cyclones," *Radio Sci.*, vol. 48, pp. 371–387, 2013, doi: 10.1002/rds.20042.

[27] E. W. Uhlhorn, P. G. Black, J. L. Franklin, M. Goodberlet, J. Carswell, and A. S. Goldstein, "Hurricane surface wind measurements from an operational stepped frequency microwave radiometer," *Monthly Weather Rev.*, vol. 135, pp. 3070–3085, 2007.

[28] E. J. Walsh, I. PopStefanija, S. Y. Matrosov, J. Zhang, E. Uhlhorn, and B. Klotz, "Airborne rain-rate measurement with a wide-swath radar altimeter," *J. Atmos. Ocean. Technol.*, vol. 31, pp. 860–875, 2014.

[29] E. J. Walsh *et al.*, "The Southern Ocean Waves Experiment. Part III: Sea surface slope statistics and near-nadir remote sensing," *J. Phys. Oceanogr.*, vol. 38, pp. 670–685, 2008, doi: 10.1175/2007JPO3771.1.

[30] J. L. Garrison, A. Komjathy, V. U. Zavorotny, and S. J. Katzberg, "Wind speed measurement using forward scattered GPS signals," *IEEE Trans. Geosci. Remote Sens.*, vol. 40, no. 1, pp. 50–65, Jan. 2002.

[31] M. Grant, S. T. Acton, and S. Katzberg, "Terrain moisture classification using GPS surface-reflected signals," *IEEE Geosci. Remote Sens. Lett.*, vol. 4, no. 1, pp. 41–45, Jan. 2007.

[32] P. Misra and P. Enge, *Global Positioning System: Signals, Measurements, and Performance*. Lincoln, MA, USA: Ganga-Jamuna Press, 2001.

[33] K. Borre, D. M. Akos, N. Bertelsen, P. Rinder, and S. H. Jensen, "A software-defined GPS and Galileo receiver: A single-frequency approach," in *Applied and Numerical Harmonic Analysis*. Boston, MA, USA: Birkhäuser, 2007.

[34] N. Rodriguez-Alvarez, D. M. Akos, V. U. Zavorotny, J. A. Smith, A. Camps, and C. W. Fairall, "Airborne GNSS-R wind retrievals using delay-Doppler maps," *IEEE Trans. Geosci. Remote Sens.*, vol. 51, no. 1, pp. 626–641, Jan. 2013.

[35] HWind data, Newark, CA, USA, 2018. [Online]. Available: http://www.hwind.co/legacy_data/

[36] V. U. Zavorotny and A. G. Voronovich, "Scattering of GPS signals from the ocean with wind remote sensing application," *IEEE Trans. Geosci. Remote Sens.*, vol. 38, no. 2, pp. 951–964, Mar. 2000.

[37] T. Elfouhaily, B. Chapron, K. Katsaros, and D. Vandemark, "A unified directional spectrum for long and short wind-driven waves," *J. Geophys. Res.*, vol. 102, no. C7, pp. 15781–15796, 1997.

[38] International GNSS Service, 2018. [Online]. Available: https://igscb.jpl.nasa.gov/

[39] C. W. Wright *et al.*, "Hurricane directional wave spectrum spatial variation in the open ocean," *J. Phys. Oceanogr.*, vol. 31, pp. 2472–2488, 2001.

[40] E. J. Walsh *et al.*, "Hurricane directional wave spectrum spatial variation at landfall," *J. Phys. Oceanogr.*, vol. 32, pp. 1667–1684, 2002.

[41] C. W. Wright *et al.*, "Measuring storm surge with an airborne wide-swath radar altimeter," *J. Atmos. Ocean. Technol.*, vol. 26, pp. 2200–2215, 2009.

[42] I.-J. Moon, I. Ginis, T. Hara, L. H. Tolman, C. W. Wright, and E. J. Walsh, "Numerical simulation of sea surface directional wave spectra under hurricane wind forcing," *J. Phys. Oceanogr.*, vol. 33, pp. 1680–1706, 2003.

[43] I.-J. Moon, I. Ginis, and T. Hara, "Effect of surface waves on air-sea momentum exchange. Part II: Behavior of drag coefficient under tropical cyclones," *J. Atmos. Sci.*, vol. 61, pp. 2334–2348, 2004.

[44] S. S. Chen, W. Zhao, M. A. Donelan, and H. L. Tolman, "Directional windwave coupling in fully coupled atmosphere-wave-ocean models: Results from CBLAST-Hurricane," *J. Atmos. Sci.*, vol. 70, pp. 3198–3215, 2013.

[45] Y. Fan, I. Ginis, T. Hara, C. W. Wright, and E. J. Walsh, "Numerical simulations and observations of surface wave fields under an extreme tropical cyclone," *J. Phys. Oceanogr.*, vol. 39, pp. 2097–2116, 2009.

[46] P. A. Hwang and E. J. Walsh, "Azimuthal and radial variation of wind-generated surface waves inside tropical cyclones," *J. Phys. Oceanogr.*, vol. 46, pp. 2605–2621, 2016.

[47] A. V. Soloviev, R. Lukas, M. A. Donelan, B. K. Haus, and I. Ginis, "The air-sea interface and surface stress under tropical cyclones," *Sci. Rep.*, vol. 4, 2014, Art. no. 5306, doi: 10.1038/srep05306.

[48] Hurrikane Ike, 2018. [Online]. Available: http://fermi.jhuapl.edu/hurr/08/ike/index.html

[49] The Loop Current, 2018. [Online]. Available: http://oceancurrents.rsmas.miami.edu/atlantic/loop-current.html

Scott Gleason (M'09–SM'14) received the B.S. degree in electrical and computer engineering from The State University of New York at Buffalo, Buffalo, NY, USA, in 1992, the M.S. degree in engineering from Stanford University, Stanford, CA, USA, in 2000, and the Ph.D. degree in remote sensing using bistatic GNSS reflections from the University of Surrey, Guildford, U.K., in 2007.

He is a Project Scientist III with the University Corporation for Atmospheric Research, Boulder, CO, USA. He is a Coinvestigator of the Science Team and an Instrument Scientist for the NASA Cyclone Global Navigation Satellite System mission. He has worked in the areas of astronautics, remote sensing, and global navigation satellite systems for more than 20 years, including at NASA's Goddard Space Flight Center; Stanford's GPS Laboratory; Surrey Satellite Technology Ltd.; Concordia University, Montreal, QC, Canada; and the National Oceanography Centre, Southampton, U.K.

Valery U. Zavorotny (M'01–SM'03–F'10) received the M.Sc. degree in radio physics from Gorky State University, Gorky, Russia, in 1971, and the Ph.D. degree in physics and mathematics from the Institute of Atmospheric Physics, USSR Academy of Sciences, Moscow, Russia, in 1979.

From 1971 to 1990, he was with the Institute of Atmospheric Physics, USSR Academy of Sciences. In 1990, he joined the Lebedev Physical Institute, Moscow, Russia. He is currently a Physicist with the Earth System Research Laboratory, National Oceanic and Atmospheric Administration, Boulder, CO, USA. He is a Coinvestigator of the Science Team for the NASA Cyclone Global Navigation Satellite System mission. His research interests include the theory of wave scattering from rough surfaces, ocean and land remote sensing applications using radar, and global navigation satellite system reflection techniques.

Dennis M. Akos received the Ph.D. degree in electrical engineering from the Avionics Engineering Center, Ohio University, Athens, OH, USA, in 1997.

He is currently an Associate Professor with the Department of Aerospace Engineering Sciences, University of Colorado–Boulder, Boulder, CO, USA, with Visiting Professor appointments with Stanford University, Stanford, CA, USA. His research interests include global navigation satellite systems, software-defined radio, applied/digital signal processing, and radio frequency design.

Sara Hrbek received the M.S. degree in engineering, spacecraft, and instrumentation from Luleå University of Technology, Luleå, Sweden, in 2012, and the M.S. degree in aerospace engineering, in 2016, from the University of Colorado–Boulder, Boulder, CO, USA, where she is currently working toward the Ph.D. degree in aerospace engineering.

Her current research focuses on receiver architecture for remote sensing using GNSS.

Ivan PopStefanija (S'86–M'91) received the BSEE degree in electrical engineering and telecommunications from the University of Ljubljana, Ljubljana, Yugoslavia, in 1982, and the Ph.D. degree in electrical and computer engineering from the University of Massachusetts, Amherst, MA, USA, in 1991.

From June 1983 to August 1984, he was a Research Associate with the Institute Mihailo Pupin, Belgrade, Yugoslavia. From July 1991 to August 1996, he was a Research Engineer and Senior Research Fellow with the Microwave Remote Sensing Laboratory (MIRSL), University of Massachusetts. At MIRSL, he specialized in the area of high-speed data acquisition and the use of multifrequency microwave radars to remotely sense ocean surface currents. He was involved in development of key instruments for use in the international SAXON-FPN and SAXON-CLT experiments. Since 1992, he has been with the ProSensing Inc. (formerly Quadrant Engineering), Amherst, MA, USA. From 1993 to 1996, he was a President of Quadrant Engineering. In 2000, with two other partners, he founded ProSensing Inc., a firm that specializes in custom-built radar and radiometer systems for a wide range of environmental remote sensing applications. At ProSensing Inc., he is a Managing Partner and a Principal Investigator on a number of projects. Over the years, he developed the data acquisition and real-time processing systems for several remote sensing instruments, including high-resolution polarimetric millimeter-wave cloud profiling radars and a modified military phased array radar to be used for severe weather surveillance. He led the development of remote sensing instruments such as the airborne combined C-band scatterometer and Doppler wind profiler and the wide swath radar altimeter for measuring directional ocean wave spectra.

Edward J. Walsh (M'74–SM'03) received the B.S. and Ph.D. degrees in electrical engineering from Northeastern University, Boston, MA, USA, in 1963 and 1967, respectively.

From 1967 to 1970, he was with the National Aeronautics and Space Administration (NASA) Electronics Research Center, Cambridge, MA, USA, both as a civil servant and while on active duty in the U.S. Army as a Captain in the Signal Corps. From 1970 to 2009, he was with the NASA Wallops Flight Facility, Goddard Space Flight Center, involved in radar remote sensing of the sea. From 1982 to 2009, he was on assignment for NASA at what is now the National Oceanic and Atmospheric Administration Earth System Research Laboratory, Boulder, CO, USA. Since retiring from NASA, he has maintained an affiliation with NOAA/ESRL, using the NOAA wide swath radar altimeter to measure sea–surface roughness, directional wave spectra, and rain rate in hurricanes. He is an author of 92 peer-reviewed articles.

Dr. Walsh was the recipient of the NASA Medal for Exceptional Scientific Achievement in 1975, and the NRL Alan Berman Research Publication Award in 2001. He is a member of Commission F of the U.S. National Committee of URSI.

Dallas Masters (M'09) received the Ph.D. degree in aerospace engineering sciences from the University of Colorado–Boulder, Boulder, CO, USA, in 2004.

He is currently the GNSS-R Product Manager with the Spire Global, Boulder, CO, USA. His research interests include satellite altimetry, passive bistatic radar remote sensing systems and analysis, scatterometry, and global navigation satellite systems.

Michael S. Grant received the M.E. and Ph.D. degrees in electrical and computer engineering from the University of Virginia, Charlottesville, VA, USA, in 2001 and 2006, respectively.

Since 1987, he has been with the NASA-Langley Research Center, Hampton, VA, USA, working in the areas of spaceflight electronics design, systems engineering, and signal processing on a number of space shuttle, aircraft-based, and satellite-based atmospheric science projects. He is currently the Langley Chief Engineer for the NASA Cyclone Global Navigation Satellite System project. His research interests include earth remote sensing, image processing, and pattern classification.